Journal of Aerosol Science 96 (2016) 24–37

Contents lists available at ScienceDirect

Journal of Aerosol Science

journal homepage: www.elsevier.com/locate/jaerosci

# Lung-deposited surface area concentration measurements in selected occupational and non-occupational environments

Otmar Geiss*, Ivana Bianchi, Josefa Barrero-Moreno

*European Commission, Joint Research Centre, Institute for Health and Consumer Protection, Via E. Fermi, 2749, 21027 Ispra, VA, Italy*

ARTICLE INFO

*Article history:*
Received 1 December 2015
Received in revised form
16 February 2016
Accepted 27 February 2016
Available online 10 March 2016

*Keywords:*
Lung-deposited surface area
Diffusion chargers
Occupational environments
Chamber studies
LDSA

ABSTRACT

Previous experimental and epidemiologic studies suggested that exposure to ultrafine particles (UFP) may result in adverse health effects. Metrics such as the number-concentration and especially the surface-area or lung-deposited surface area (LDSA) appear to be appropriate metrics of dose for predicting pulmonary inflammation of insoluble and poorly soluble ultrafine particles. Currently not much data including LDSA concentrations is available. The aim of this study was therefore to measure LDSA concentrations in a variety of occupational and non-occupational environments as well as in chamber tests. To this end, novel handheld online-monitors were deployed and evaluated for their suitability to be used in a variety of micro-environments and under different conditions. Chamber emissions tests included incense and candle burning, 3D printing and cigarette/e-cigarette smoking. The LDSA concentration was measured in occupational environments such as a canteen kitchen, a welding workshop and in a car. Measurements were also conducted in a private house with a wood-burning stove and with ongoing parallel cooking activities. Depending on the type of micro-environment, the ongoing activities or the material investigated in the chamber-tests, large differences were observed in terms of measured LDSA concentrations, some exceeding up to 1000 times that of the baseline concentration detected before activities initiated. In some of the investigated environments LDSA concentrations were measured for the first time. The data might therefore serve as reference for future studies. The handheld instrument used to measure this data worked well both for stationary measurements as well as for personal monitoring and proved to be an alternative to bulkier benchtop instruments.


## 1. Introduction

Experimental and epidemiologic studies conducted in the past indicated that exposure to ultrafine particles (UFP) may result in adverse health effects (Hoek et al., 2010; Mills et al., 2009; Rückerl, Schneider, Breitner, Cyrys, & Peters, 2011). Currently there is however no common agreement on an appropriate metric of exposure for ultrafine particles.

Exposure to coarse airborne particles has typically been assessed by measuring the mass-concentration. For ultrafine particles however, other metrics such as the number-concentration and especially the surface-area seem to be more appropriate metrics of dose for predicting pulmonary inflammation caused by insoluble and poorly soluble particles (Aitken, Chaudhry, Boxall, & Hull, 2006; Oberdorster, Oberdorster, & Oberdorster, 2005; Sager & Castranova, 2009; Waters et al.,

* Corresponding author. Tel.: +39 0332 786323; fax: +39 0332 786012.
*E-mail address:* otmar.geiss@ec.europa.eu (O. Geiss).

http://dx.doi.org/10.1016/j.jaerosci.2016.02.007

2009). The Scientific Committee on Emerging and Newly Identified Health Risks (SCENIHR, 2006) concluded in its 'opinion on the appropriateness of existing methodologies to assess the potential risk associated with engineered and adventitious products of nanotechnologies' that for exposure evaluation, dose requires information on the number of nanoparticles and/or their surface area in addition to traditional mass concentration characterization and that the equipment used for routine measurements, in various media, for representative exposure to free nanoparticles is currently inadequate. Surface area reflects the surface of particles, but can be interpreted in several ways. Which surface area (geometric surface area, Brunauer-Emmett and Teller (BET) surface area, active surface area) is the most relevant depends on the fact that which information is important for the user. The BET surface area (Brunauer, Emmett, & Teller, 1938) measurement technique, for instance, which relies on the absorption of gases on the particles surface can only be applied for powders and moreover measurements are influenced by particle porosity. The geometric surface area can be calculated through the particle number-size distribution, assuming perfect sphericity of particles. The active or 'Fuchs' surface area of aerosols can be determined with an epiphaniometer by measuring the attachment rate of radioactive ions to the sampled particles. The necessity of a radioactive source makes this technique less attractive for widespread use. An alternative to measuring the total surface area is measuring the lung-deposited surface area (LDSA) concentration instead which can be more easily measured. This metric takes into account the deposition efficiency of particles in different compartments of the lung based on a model published by the International Commission for Radiological Protection and defined for a reference working person (ICRP, 1994). LDSA concentration can be measured with so-called 'unipolar diffusion chargers' which are based on the same measurement principle as the epiphaniometer but without the requirement of a radioactive source. They consist of 3 basic elements: the unipolar charger (usually a corona charger), where ions are generated and mixed with the particles to charge them, the ion trap, where excess ions are removed, and finally a filter, where all particles are captured and the current deposited by the particles onto the filter is detected with a sensitive electrometer. It has been shown that, following unipolar diffusion charging, the resulting charge level of an aerosol is proportional to the fraction of the particle surface area concentration that would deposit in either the alveolar (gas-exchange) or the thoracic region of the human lungs. This relationship does however only apply in the size-range 20–400 nm (Asbach, Fissan, Stahlmecke, Kuhlbusch, & Pui, 2009; Kaminski et al., 2012). In a recent study, Todea et al. (Todea, Beckmann, Kaminski, & Asbach, 2015) determined the accuracy of instruments measuring the alveolar LDSA concentration based on unipolar diffusion charging and found that the measured concentrations were within 30% of accuracy in the size-range 20–400 nm. Provided the majority of particles are in this range of size, it is therefore possible to directly determine the LDSA concentration with unipolar diffusion chargers such as those used in this study.

Generally, little data, including LDSA concentrations, is available. Ambient LDSA background concentrations were measured in a number of national measuring campaigns e.g. in Switzerland (Eeftens et al., 2015), Barcelona (Reche et al., 2015), Lisbon (Gomes, Bordado, & Albuquerque, 2012) and Como (Spinazzè, Cattaneo, Scocca, Bonzini, & Cavallo, 2015). Other studies related the active surface of particles to spirometric results on 7–10 year old children in Upper Austria (Moshammer & Neuberger, 2003), quantified exposure to particles emitted by wood-fire ovens in pizzerias (Buonanno, Morawska, Stabile, & Viola, 2010), determined real-time individual exposure of more than 100 children aged 8–11 years during typical school days to particle number concentrations and average particle diameter, as well as alveolar and tracheobronchial deposited surface area concentration (Buonanno, Marini, Morawska, & Fuoco, 2012).

The aim of this study was to measure current scarcely available LDSA concentrations in a variety of occupational and non-occupational environments as well as during emission chamber tests. To this end novel handheld online monitors were deployed and evaluated on their suitability to be used in a variety of micro-environments and under different conditions. In a number of selected environments, the LDSA was measured for the first time and could therefore serve as a reference for future studies.

## 2. Materials and methods

### 2.1. Instrumentation

#### 2.1.1. Lung-deposited surface area

Two commercially available instruments, based on the diffusion charging principle, were used in this study.

*2.1.1.1. Aerotrak 9000.* The Aerotrak Nanoparticle Aerosol Monitor 9000 (TSI Incorporated, Shoreview, USA) measured the LDSA concentration with 1-second resolution and an inlet flow of 2.5 L $min^{-1}$. Particles larger than 1 μm are removed by a cyclone. The voltage of the ion trap can be changed to adjust the instrument's response to either alveolar or tracheobronchial LDSA concentrations. The concentration range (alveolar) is advertised by the manufacturer as being 1–10,000 $\mu m^2\ cm^{-3}$. This instrument has been extensively characterised in previous studies (Asbach et al., 2009; Bau, Witschger, Gensdarmes, & Thomas, 2012; Fissan, Neumann, Trampe, Pui, & Shin, 2007; Leavey, Fang, Sahu, & Biswas, 2013; Shin, Pui, Fissan, Neumann, & Trampe, 2007).

*2.1.1.2. Partector.* The Partector (Naneos Particle Solutions GmbH, Windisch, Switzerland) is a small, light (400 g) battery-operated personal monitor (Fierz, Meier, Steigmeier, & Burtscher, 2013) which measures the alveolar LDSA concentration

with a 1-second resolution. The sample flow was 0.5 L $min^{-1}$. The concentration range is advertised by the manufacturer as being 1–20,000 $\mu m^2$ $cm^{-3}$. To date this instrument has only been used in very few laboratory studies (Todea et al., 2015).

*2.1.2. Particle number concentration*

A recent study (Todea et al., 2015) demonstrated that the LDSA concentration can be measured with sufficient accuracy as long as the vast majority of particles are within a size range of 20–400 nm. As the LDSA concentration instruments used in this study do not provide information on the number-size distribution, where physically possible, complementary (in parallel) measurements providing number-size distribution information in two size ranges (20–300 nm and $>300$ nm) were conducted. For this purpose two types of real-time laser photometers were used. Particles with an optical equivalent particle size range of $>0.3$ μm were measured using a GRIMM model 1.108 portable optical particle counter (GRIMM Aerosol Technik GmbH & Co. KG, Ainring, Germany). Those with an optical equivalent particle size range of 0.02–1 μm were measured using a P-Trak® ultrafine particle counter (TSI Model 8525, TSI Incorporated, Shoreview, USA), an instrument based on the condensation particle counting technique using isopropyl alcohol. Both instruments were calibrated by the manufacturers against certified calibration standards: the P-Trak against the PortaCount Bench 1 calibration standard and the GRIMM against Arizona Test Dust (ISO 12103-1, 1997). Data collection frequency was one point per minute.

*2.1.3. Test chamber*

A 30 $m^3$ walk-in environmental chamber was used in this study. The chamber allowed precise control of temperature, relative humidity and air exchange rate. The air exchange rate was set by introducing defined volumes of air per unit of time and this was verified by means of tracer gas dilution tests using sulphur hexafluoride (ASTM, 2011). Using only stainless steel, glass and 'non-stick' poly-tetrafluoroethylene (PTFE) polymer coatings in the interior of the chamber minimised pollutant adsorption and re-emission by the inner walls. The chamber was filled with ultra-clean pre-dried and filtered air and it was run at an air exchange rate of 0.5 $h^{-1}$ to realistically simulate an indoor environment. The temperature was set at 23 °C and the relative humidity at 50%. Homogeneity of the atmosphere inside the chamber was ensured by three internal fans. The chamber air was aspirated by the instrument through an antistatic tube approximately 1 m long.

*2.2. Comparison of lung-deposited surface area concentrations measured with the Aerotrak 9000 and with the Partector*

In most of the measurements conducted in this study, both the Aerotrak and Partector were used in parallel thus allowing direct comparison of the collected data. For this purpose, both instruments were set for the measurement of alveolar LDSA concentrations.

*2.3. Description of investigated environments and tested materials*

*2.3.1. Determination LDSA-concentrations in normally polluted ambient and indoor environments (determination of reference baseline values)*

As the LDSA is a relatively unfamiliar metric, with very little data available to date, the purpose of these measurements was to determine average ambient and indoor LDSA concentrations in 'normally polluted' environments against which all other measurements, collected in this study, may be compared. This was done by measuring the LDSA concentration over 26 days distributed between April and July 2015. Concentrations were averaged over a 5 min period, always at the same time (around 10 a.m.), and collected in the same place (indoors: average office with no particular sources for particles and outdoors: in front of the building hosting the office in which indoor measurements were carried out). The location was Ispra (VA), Italy: an area of low traffic density.

*2.3.2. Chamber tests*

The following objects were placed in the centre of the chamber. The chamber was operated as described in Section 2.1.3.

*2.3.2.1. 3D-printer.* The vast majority of commercially available 3D printers operate based on molten polymer deposition technique (MPD). A solid thermoplastic filament is pushed through a hot extrusion nozzle which melts the filament and deposits streams of extruded polymer in thin layers across a moving sample platform. The printer used for this test (SD. 1) was a single nozzle XYZ Printing da Vinci 1.0 (XYZ printing San Diego, CA, USA) and the printing technology used is based on fused filament fabrication (FFF). The nozzle diameter was 0.4 mm and the filament diameter 1.75 mm. The printer case was generally closed except for two lateral apertures each of approximately $(16 \times 4)$ $cm^2$. The filament material was acrylonitrile butadiene styrene (ABS). The nozzle temperature and the platform temperature were 214 °C and 90 °C, respectively. The printed object (SD. 1) was chosen based on criteria such as duration of the printing process and likelihood that the printing process would be discarded due to unexpected errors. From the moment the printing command was given to the 3-D printer, the nozzle and the sampling plate were heated up to their respective end-temperatures. This step lasted approximately 8 min. The object itself was printed in approximately 53 min and weighed approximately 9 g.

*2.3.2.2. Incense.* The incense used in this study was a direct-burning incense (or “combustible incense”) which was lit directly by a flame leaving a glowing ember that smouldered and released fragrance. Incense paste extruded into a cone

**Table 1**
Smoking parameters set on the smoking machine for traditional and electronic cigarettes.

| Parameter | Traditional cigarette | E-cigarette |
|---|---|---|
| Puff-volume | 35 mL | 50 mL |
| Puff-duration | 2.0 s | 3.0 s |
| Puff-number | 6 (butt-length: 35 mm) | 15 |
| Intermission | 60 s | 30 s |
| Puff-profile | bell-shaped | bell-shaped |

shape (SD. 1) was preferred over the more frequently used bamboo stick type with the paste formed around it, as emissions from the burning bamboo-stick could influence the particles emitted. The cones were sold in a set, which was made in China and labelled "Colorado Aromatic Candle", including scented candles and incense covered bamboo-sticks. The initial weight of each cone was approximately 0.94 g. The glowing process lasted approximately 10 min. The incense cone was placed in a glass container (SD. 1) which was located on the floor in the centre of the chamber. The cone was manually lit with a cigarette lighter.

*2.3.2.3. Candle.* The white candle used in this study was made of refined paraffin (Candele Tuttigiorni, Magic Lights Srl, Beinasco-TO, Italy) and was labelled by the manufacturer as it did not contain toxic ingredients. The candles were 16 cm long and 2 cm in diameter. For conditioning purposes, the candle was lit for 5 min before the measurement started. Before placing the candle into the emission chamber, it was extinguished again and cooled to room temperature. The candle was then transferred to a glass beaker to avoid dripping of the wax on the floor of the emission chamber. During the emission test, the flame of the candle was always above the edge of the beaker (SD. 1) thus allowing regular, unhindered burning. After lighting the candle for approximately 90 min, it was removed from the chamber without extinguishing it to avoid smoke peaks. In total, 9.95 g of candle-material were consumed during the experiment.

*2.3.2.4. Tobacco cigarette and electronic cigarette.* Both the traditional and the electronic cigarette were smoked/vaped with a smoking machine. The smoking machine used was a single channel Borgwaldt RM-1 Plus smoking machine (Borgwaldt KC GmbH, Hamburg, Germany). In the case of the traditional tobacco cigarette the smoking parameters were adapted to standard conditions as defined in ISO 3308 (ISO 3308, 2012). In the case of the e-cigarette, the standard conditions were adapted according to the findings of Behar et al. (Behar, Hua, & Talbot, 2015) who investigated the puffing topography and nicotine intake of electronic cigarette users (Table 1).

a) *Traditional (tobacco) cigarette*: the smoking machine was placed inside the emission chamber (SD. 1). One Marlboro Gold cigarette (8 mg tar, 0.6 mg nicotine and 9 mg carbon monoxide) was smoked.
b) *E-cigarette*: the type of electronic cigarette used in this study was a third-generation product ("Mod") composed of two separately purchased components: the battery and the atomizer. The battery was a 2200 mAh battery (Eleaf, ISTICK, 30 W, Ismoka, China) providing a variable output voltage/wattage range of 2 V-8 V/5 W-30 W. The atomizer was a Kayfun 3.1 (EHPRO, China) re-buildable bottom coil atomizer with an adjustable airflow. The amount of airflow going to the coil was set at 50% aperture. The transparent tank had a capacity of approximately 4.5 mL. An 11 cm long Nichrome 80 type (0.3 mm diameter) wire was used to wrap the coil (11 wraps). The resistance of this coil corresponded to approximately 1.6 Ω. The e-liquid used in this study (Heaven Juice Traditional Tobacco 7 Leaves) was purchased, over the internet, from one of the principal e-cigarette refill liquid retailers in Italy (Flavourart srl, Oleggio (NO), Italy) and was composed of glycerol (50%), propylene glycol (40%), water (6%), tobacco fragrance (3%) and nicotine (0.9%).

The smoking machine was placed outside the chamber as the operation of the e-cigarette had to occur manually. Keeping the glass fibre filters in line between the e-cigarette and the piston of the smoking machine and introducing the exhaust of the smoking machine into the chamber would have altered the vapour composition. Removing the filters would have led to contamination of the piston and pneumatic valves resulting in potential pollutant carry-over. For this purpose an empty gas washing bottle, of 500 mL volume, was placed between the e-cigarette and the smoking machine (SD. 2) and the puff volume was calibrated where this was connected to the e-cigarette. A volume of 500 mL was chosen, as this proved sufficient to contain the whole of each 35 mL puff volumes without any loss. At the end of each puff, all vapour trapped inside the bottle was removed by flushing it with a strong ( $> 30$ L min$^{-1}$) flow of nitrogen for approximately 5 s and conducted into the chamber.

*2.3.3. Measurements in occupational environments*
*2.3.3.1. Car journey.* Lung-deposited surface area (LDSA) concentration was measured during a car journey from Turin to Borgomanero, in northern Italy (SD. 1). The overall distance was 106 km and the journey had a duration of 1 h and 22 min. Windows were kept closed and ventilation was set at "fresh air" mode. The journey took place in the evening from approximately 8 p.m. to 9:22 p.m. on the 9th of April 2015. The outside temperature was around 25 °C. Weather conditions were good.

*2.3.3.2. Canteen kitchen.* Approximately 1000–1500 meals are daily prepared in this kitchen. Although the menu changes, the main operations are roughly the same every day: as a first step, at around 7 a.m. the kitchen staff starts cutting vegetables and preparing other ingredients. At around 8 a.m. the gas stoves and, at around 10:30 a.m., the fryers are turned on. Meals are served from 11 a.m. to 2 p.m. Data was collected over the whole duration, from around 7 a.m. to around 2:15 p.m. Instruments were placed on a shelf close to one of the walls at a height of approximately 2 m (SD. 1). The area of the kitchen is approximately 140 $m^2$ with a ceiling height of approximately 2.5 m.

*2.3.3.3. Welding.* Welding is a process that joins materials, usually metals, through fusion, which is distinct from lower temperature metal-joining techniques such as brazing and soldering, which do not melt the base metal. In addition to melting the base metal, a filler material is often added to the joint to form a pool of molten material (the weld pool) that cools to form a joint that can be as strong as the base material. The welding method under investigation here was 'gas tungsten arc welding' (GTAW) – also known as TIG (tungsten inert gas) which uses a non-consumable tungsten electrode to produce the weld. The weld area is protected from atmospheric contamination by an inert shielding gas (in this case Argon). The filler material (filler rod) was Inox 308 steel and the base-metal Inox 304 steel. Data was collected during 30 min of welding. The welding was done in a mechanic's workshop (SD. 1) with an area of approximately 2500 $m^2$ and 15 m of height. Adjacent (10 m distance) to the welding station, there was a construction site in which combustion engines were discontinuously operating. For this reason the background particles concentration was already higher than usual. A Partector and the Aerotrak 9000 together with the P-Trak and the Grimm were placed on a shelf approximately 2 m from the welding station. In addition to these stationary measurements, the welder wore a second Partector instrument on his belt which aspirated air from the breathing zone (SD. 1). Two welding-sessions were monitored, the first starting at 9:02 a.m. and ending at 9:20 a.m. and the second starting at 9:28 a.m. and ending at 9:34 a.m.

*2.3.4. Other measurements*

*2.3.4.1. Private house with wood-burning stove.* Measurements were conducted in the living room of a private house while a wood-burning stove was lighting. The living room had a floor area of approximately 50 $m^2$ and a height of 2.7 m, resulting in a volume of approximately 135 $m^3$. Samples were collected at a distance of approximately 2 m from the stove (SD. 1). The peculiarity of this type of stove is that its door has to be opened each time a new billet of wood is added. This operation potentially releases smoke into the environment. In addition, if during the ignition phase the fire does not immediately light, the door needs to be opened again causing the smouldering fire to release smoke into the environment. In this experimental setup, particulate measurements were started approximately 20 min before igniting the fire and for approximately 3 h while the stove was operational. Measurements were conducted during the evening (6–9 p.m.). During the measurement period, preparation of dinner (only boiling of water) took place in an open space kitchen adjoining the living room (SD. 1). The gas cooker, which was used to boil the water, was lit for approximately 15 min.

## 3. Results

### 3.1. Comparability of data recorded with the Aerotrak and with the Partector

Approximately 2600 data points were simultaneously collected and plotted against each other. The result is depicted in Fig. 1.

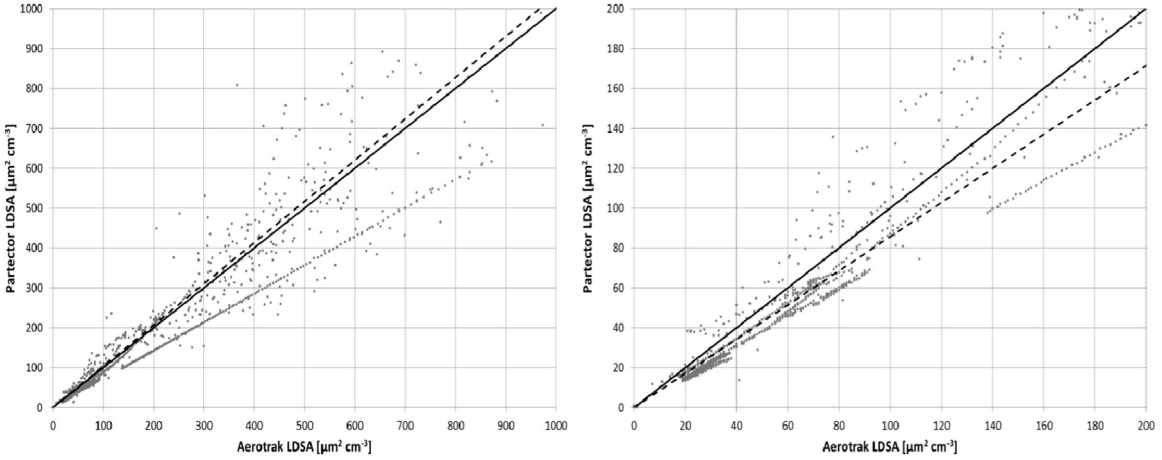


**Fig. 1.** Lung-deposited surface area concentrations collected with the Aerotrak plotted against those collected with the Partector. Left: all data points covering the whole concentration range. Right: only concentrations below 200 $\mu m^2\ cm^{-3}$ (continuous line: $x=y$; dashed line: regression line).

Over the whole concentration range (Fig. 1, left), the regression line (dashed) is in good agreement with the continuous $x=y$ line. If all data points exceeding 200 $\mu m^2\ cm^{-3}$ are however removed (remaining data points $n=2200$) the regression line moves below the $x=y$ line (Fig. 1, right). Approximately 85% of all collected data points fell into this second concentration range, where the concentration data measured with the Partector are 15% lower than those collected with the Aerotrak. This finding is in agreement with Todea et al. (Todea et al., 2015) who compared a number of diffusive chargers against mono-disperse model test aerosols and found the Partector to slightly underestimate and the Aerotrak to slightly overestimate the test aerosol concentration. The good agreement between the concentrations measured using both instruments shows that the handheld Partector is a valid alternative to the much bulkier Aerotrak 9000. This is particularly relevant where small dimensions and/or low-weight are a prerequisite for the successful execution of the measurement (e.g. in personal monitoring).

### *3.2. Repeated indoor/outdoor measurements – determination of indoor and outdoor reference baseline values for 'normally' polluted environments*

A total number of 26 parallel indoor/outdoor measurements were conducted on separate days. Results show that outdoor LDSA concentrations are generally higher (I/O ratio=0.7) and have a higher variability. Average concentrations of $23 \pm 8.4\ \mu m^2\ cm^{-3}$ and $16.9 \pm 6.0\ \mu m^2\ cm^{-3}$ were measured outdoors and indoors respectively. A number of studies conducted in the past measured the LDSA concentration outdoors; Reche et al. (2015) found average ambient air concentrations of $37 \pm 26\ \mu m^2\ cm^{-3}$ in the city of Barcelona, Eeftens et al. (2015) measured LDSA concentrations in various outdoor sites in Switzerland and found an average concentration of around 30 $\mu m^2\ cm^{-3}$, Gomes et al. (2012) measured LDSA concentrations in the city of Lisbon and found concentrations ranging from 35 to 90 $\mu m^2\ cm^{-3}$. Due to the rural location in which the data were collected in this study, the value of 23 $\mu m^2\ cm^{-3}$ is slightly lower compared to the values found in the studies listed above. For comparison purposes, these values can be used as reference values for a normally (low) polluted indoor environment and for ambient air.

### *3.3. Chamber tests*

#### *3.3.1. Particulate emissions during operation of 3D-printer*

From the moment the printing command was sent from the computer to the printer, the nozzle and the sample plate were brought to their operational temperatures. This process took approximately 8 min. During this first phase a fan, located at the bottom left side of the printer, (SD.1) was automatically and irregularly activated to compensate for the heating-up of the nozzle and sample, to speed up the heating process to the operational temperatures (214 °C the nozzle and 90 °C the sample plate). This phase is marked with the letter B in Fig. 2. A strong formation of particles can be observed already in this phase. The heating up of ABS seems to lead to a formation of particles which are emitted from the printer case through the ventilator.

In the second phase the effective printing started and Fig. 2 shows how the formation rate of particles did not significantly change compared to the first phase. The steady-state plateau was reached after approximately 40 min after the printing process began. From the plateau, the particles emission rate can be calculated. The emission rate is defined as the total emitted particles per hour and is calculated according to Eq. (1) where $c$ is the measured particle number-concentration in the chamber:

$$\mathrm{ER}\left[\#\ \mathrm{h}^{-1}\right] = c\left[\#\ \mathrm{m}^{-3}\right] \times \text{ chamber volume}\left[\mathrm{m}^3\right] \times \text{ air exchange rate}\left[\mathrm{h}^{-1}\right] \quad (1)$$

The calculated emission rate for particles in the size range 20–300 nm was approximately $6.3 \times 10^{11}$ particles per hour. Only one comparable study has been conducted in the past by Stephens et al. (Stephens, Azimi, El Orch, & Ramos, 2013) who measured ultrafine particle emissions from 3D printers – using both PLA and ABS feedstock – in a 45 $m^3$ furnished office space. They calculated an emission rate of $1.8–2.0 \times 10^{11}$ particles $min^{-1}$ for using the higher temperature ABS feedstock. This value is approximately 18 times higher than the findings in this study. The reason might be that the size range of particles used for calculating the emission rate is not exactly the same (this study: 20–300 nm; Stephens et al.: 11.5–116 nm) and the experimental setup also differed between the studies.

In this study, the printed test object, (SD. 1), had a weight of approximately 9 g. The emission rate could therefore also be expressed as $7 \times 10^{10}$ particles emitted per g of printed object or resin processed.

Evaluation of the data collected with both the condensation particle counter (CPC) and the optical particle counter (OPC) demonstrated that almost the all ( > 99%) of the particles were in the size range of between 20 and 300 nm. This is in good agreement with the findings of Stephens et al. (2013) who measured particle number concentrations with a scanning mobility particle sizer (SMPS) across 13 bins from 10 to 420 nm and observed no formation of particles larger than 116 nm. The LDSA measured by both the Aerotrak and the Partector are generally in good agreement and reached area concentrations of up to approximately 65 $\mu m^2\ cm^{-3}$ starting from a baseline concentration of approximately zero $\mu m^2\ cm^{-3}$. Only at higher surface areas ( > 60 $\mu m^2\ cm^{-3}$) did the Partector measure approximately 15% lower concentrations.

Studies on high-temperature thermal processing of thermoplastics, conducted in the past, on industrial extrusion equipment showed that both gases and particles are emitted by this process (Contos et al., 1995; Unwin, Coldwell, Keen, &

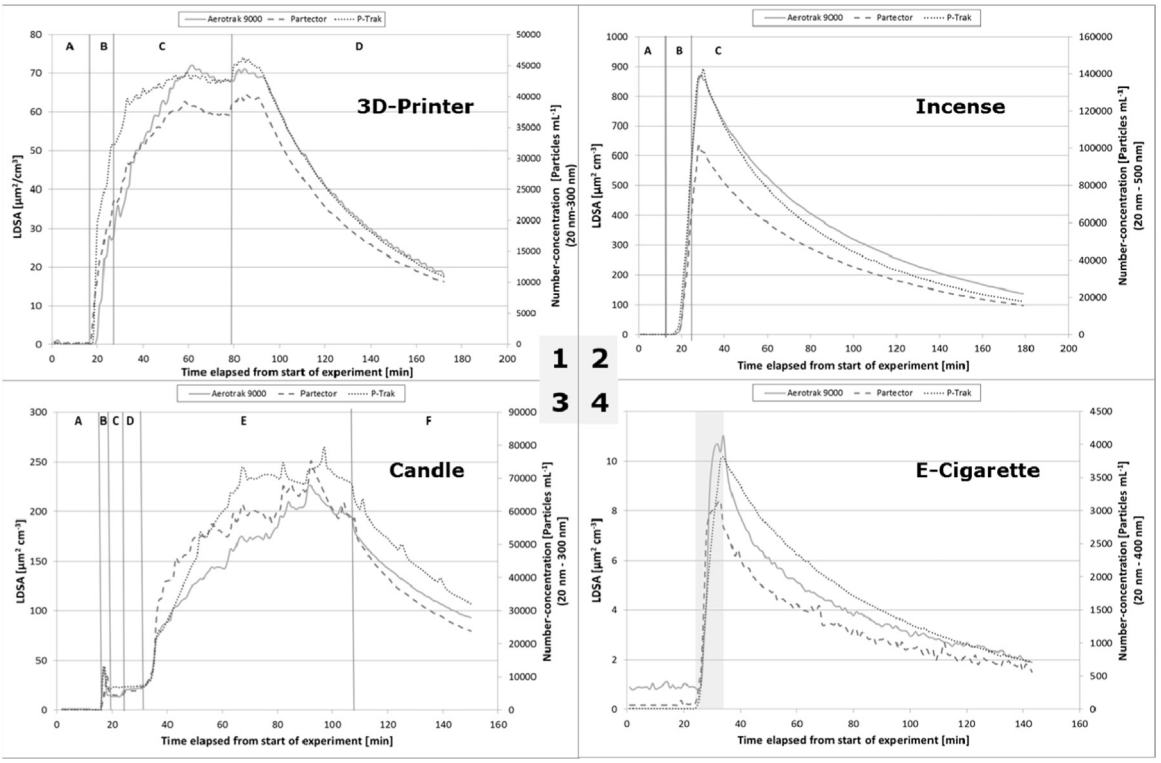


**Fig. 2.** Chamber tests. Lung-deposited surface area- and number-concentration of particles emitted from a (1) 3D-printer during the printing process. (A=baseline recording before start of experiment; B=heating up of nozzle and sample plate; C=printing process ongoing; D=end of printing. Cooling down of nozzle and sample plate), (2) glowing incense cone (A=baseline recording before start of experiment; B=glowing of cone; C=cone finished to glow), (3) burning candle. (A=baseline recording before start of experiment; B=ignition of candle; C and D=melting of paraffin; E=burning of paraffin; F=end of experiment) and (4) an electronic cigarette (the shaded section represents the vaping interval).

McAlinden, 2013). According to Morawska et al. (2009) condensation of synthetic organic vapours (VOC) from the thermoplastic feedstock is likely to be the main formation process for ultrafine particles. ABS is generally a low-hazard material and presents few health risks. However, in some situations, precautions are advisable: heating up ABS during production (as in 3D printing) can produce fumes of acrylonitrile. There is a concern that acrylonitrile could be a human carcinogen. Sealed special boxes with powerful air funnels and remote controlling of the process can mitigate the risks associated with the use of ABS.

### 3.3.2. *Particulate emissions from incense burning*

The emission profile (Fig. 2) shows a steeply increasing concentration of particles during the 10 min the incense cone was glowing (section B). During this relatively short glowing time, steady-state conditions were not reached. However, at the end of the glowing period, peak LDSA concentrations of approximately 900 $\mu m^2\ cm^{-3}$ and 600 $\mu m^2\ cm^{-3}$ were detected by the Aerotrak 9000 and the Partector respectively. A particle number-concentration of approximately 140,000 particles $mL^{-1}$ was measured. Ji et al. (2010) characterized particles emitted by incense burning in an experimental house and found approximately 50,000 particles $cm^{-3}$ and a LDSA of approximately 500 $\mu m^2\ cm^{-3}$ (values normalised to a room-volume of 30 $m^3$). The slightly higher air renewal rates and higher sink-rates in their study might explain the differences. Although steady-state conditions were not reached, the 'lowest' emission rate for particles in the size-range 20–500 nm, calculated according to Eq. (1), using the peak concentration reached at the end of the glowing phase, revealed values of $2.1 \times 10^{12}$ particles $h^{-1}$. Emitted particles were all in the size-range of 20–500 nm with the almost all ( > 99%) below 300 nm. This is in good agreement with previous studies; (Chang, Lee, & Tseng, 2007; Chuang, BéruBé, Lung, Bai, & Jones, 2013; Ji et al., 2010; Stabile, Fuoco, & Buonanno, 2012) who all investigated particle emissions from different types of incense under varying experimental conditions (e.g. relative humidity) and found number and size distributions ranging from 20 nm to 500 nm with median diameters of around 100–200 nm. Incense is composed of aromatic plant materials, often combined with essential oils. The combustible base of a direct burning incense mixture not only binds the fragrant material together but also allows the produced incense to burn with a self-sustained ember, which propagates slowly and evenly through an entire piece of incense with such regularity that it can be used to mark time. The base is chosen such that it does not produce a perceptible smell. Chang et al. (2007) suspected nucleation and coagulation to be the principal mechanisms governing the initial formation and subsequent growth of particles, respectively. They found that incense smoke was composed primarily of oil (essential oils) droplets and solid smoke particles. Number concentration and surface area of the

particles emitted from the incense cone used in this study are only indicative as varying combinations of ingredients used and differing processing techniques are likely to influence emission patterns.

### 3.3.3. Particulate emissions from candle burning

The particles emissions profile in Fig. 2 shows 4 sections in addition to the initial baseline recording and the final ventilation section. At the ignition of the candle (section B), using a cigarette lighter, a first emission peak appears which can very likely be attributed to smoke generation due to incomplete combustion processes occurring during the ignition of the candle. This peak is followed by two plateaus (sections C & D) which might be attributable to the phase where most of the flames' energy is invested in the melting of paraffin. At the end of this section equilibrium between molten and burning paraffin is reached. In the following section (section E), a strong increase in emitted particles can be observed. Fluctuations are caused by unsteady burning (flickering) of the flame. Steady-state conditions are reached after approximately one hour and under these conditions an LDSA concentration of approximately 220 $\mu m^2\,cm^{-3}$ and a particle number concentration (20–300 nm) of 74,000 particles $mL^{-1}$ were measured. According to Eq. (1) this corresponds to an emission rate of $1.11 \times 10^{12}$ particles per hour or $1.6818 \times 10^{11}$ particles per g of burned paraffin. A comparable emission rate ($2.45 \times 10^{13}$ particle $h^{-1}$) was reported by Zai et al. (Zai, Zhen, & Jia-song, 2006) in their study on size distribution, number and mass emission factors of candle particles.

All detected particles were of sizes below 200 nm which is in good agreement with previous studies (Pagels et al., 2009; Stabile et al., 2012; Zai et al., 2006) that determined median particle diameters emitted from paraffin candles of between 10 and 90 nm.

In contrast with other open combustions like wood fires in open fireplaces for example, the flame of a steadily burning candle shows very high-temperatures and, as a result, the candle wax is combusted almost completely. The undesired incomplete combustion, during which also pollutants can be emitted, can be recognized by a flickering flame or the visible release of soot. If the candle flame is not extinguished with a candle snuffer but blown out instead, there is also an incomplete combustion taking place during the short after-glowing phase. If a candle is burning with a steady flame, it emits a comparably high-number of ultrafine particles (Pagels et al., 2009). These particles are however mainly composed of inorganic water-soluble salts like phosphates, required to improve the wick performance. In addition to these ultrafine particles, sooting candles also emit bigger particles mainly consisting of elemental carbon.

### 3.3.4. Traditional tobacco cigarette and electronic cigarette

*3.3.4.1. Traditional tobacco cigarette.* The smoking process took a total time of 6 min during which time a steep increase in the concentration of ultrafine particles could be observed (Fig. 3, right). The peak concentration was reached with the sixth and last puff and corresponds to a number-concentration of approximately 165,000 particles $mL^{-1}$ and a LDSA of 1035 $\mu m^2\,cm^{-3}$ and 784 $\mu m^2\,cm^{-3}$ measured with the Aerotrak 9000 and the Partector respectively. The concentration measured with the Partector is approximately 25% lower.

Steady-state conditions were not reached while smoking only one cigarette. However, applying Eq. (1) and using the peak concentration reached after the last puff, an emission rate of $2.475 \times 10^{12}$ particles $h^{-1}$ can be calculated. This emission rate serves only for semi-quantitative comparison purposes as the real emission rate would be higher.

*3.3.4.2. Electronic cigarette.* Vaping 15 puffs took approximately 8 min and generated a concentration peak corresponding to 3800 particles $mL^{-1}$ and 10 $\mu m^2\,m^{-3}$ and 8 $\mu m^2\,m^{-3}$ LDSA measured with the Aerotrak and the Partector respectively (Fig. 3, left). Steady-state conditions were not reached while smoking only one cigarette. However, by applying Eq. (1) and using the peak-concentration reached after the last puff, an emission rate of $5.7 \times 10^{10}$ particles $h^{-1}$ can be calculated. This emission rate serves only for semi-quantitative comparison purposes as the real emission rate would be higher.

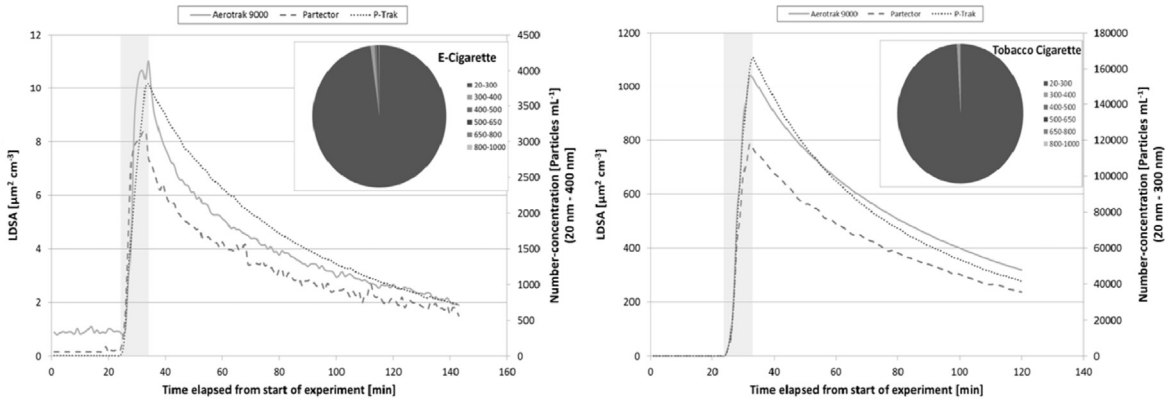


**Fig. 3.** Comparison of LDSA- and particle number-concentration emission-profile of traditional tobacco cigarette and of e-cigarette. The shaded sections represent the period when the cigarette was lit. The chart at the top-right shows the size-distribution at the concentration peak.

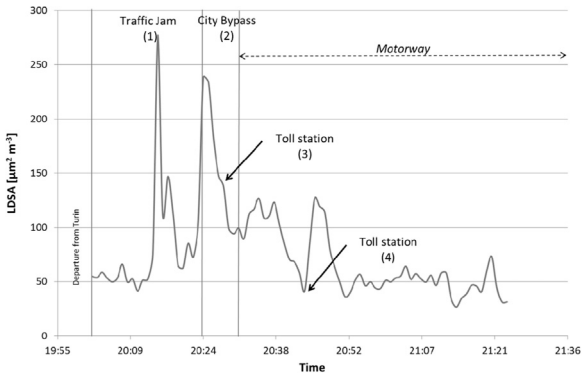


**Fig. 4.** Lung-deposited surface area concentration profile during the journey from Turin to Borgomanero.

*3.3.4.3. Comparison of emissions by tobacco cigarette and e-cigarette.* Two main differences between particulate emissions of traditional tobacco cigarettes and those of e-cigarettes were observed: (a) the total amount of generated ultrafine particles was much higher when smoking a traditional tobacco cigarette. The peak concentration exceeded approximately 43 × that of e-cigarettes in terms of number-concentration and approximately 100 × in terms of LDSA; (b) the size-distribution of particles in the emissions peak differs slightly. Particles emitted by traditional cigarettes are entirely composed of particles in the size range 20–500 nm whereas emissions by the e-cigarette generated also a small fraction of particles in the size-range 500–800 nm (Fig. 3).

In a comparable study Geiss et al. (Geiss, Bianchi, Barahona, & Barrero-Moreno, 2015) showed how the larger particles emitted by e-cigarettes very quickly deposit (and/or evaporate) and only the particles with a size below 200 nm remain suspended for a longer time. Particles emitted by traditional tobacco cigarettes have a different composition compared to those emitted by electronic cigarettes and have been demonstrated to have adverse cardiovascular and respiratory effects in human and animal models (Brook et al., 2010). The short- and longterm toxicity-potential of particles generated by electronic cigarettes is currently unknown.

### 3.4. Measurements in occupational environments

#### 3.4.1. Car journey

Figure 4 shows strong LDSA-concentration fluctuations during the ride. The route started in the city of Turin and for the first 24 min (1) the car was stuck in a traffic jam. In this part of the drive a peak LDSA-concentration of approximately 275 $\mu m^2\ m^{-3}$ was reached corresponding to 5 times the concentration measured before starting the journey. In the second section shown in Fig. 4 the traffic jam was overcome and the car was driven on a heavily trafficked city bypass road. In this section, peak LDSA-concentrations of around 230 $\mu m^2\ m^{-3}$ were reached. Once on the motorway (last section in Fig. 4), the traffic became lighter and LDSA concentrations decreased to the initial 50 $\mu m^2\ m^{-3}$. Points (3) and (4) in Fig. 4 mark the reaching of toll stations. Here the car window was opened for a short period of time resulting particularly at point (4) in a sharp LDSA-concentration increase.

Cars are equipped with particulate air filters which are composed of fibrous materials and remove solid particulates, such as dust and pollen in the micron-range, from the air. Ultrafine particles are however not retained by standard automotive air filters and thus reach the interior of the vehicle cabin. Short-term exposure to peak concentrations as those encountered during this measurement may be associated with adverse health effects (Delfino, Zeiger, Seltzer, & Street, 1998; Katsouyanni et al., 1997; Michaels and Kleinman, 2000; Peters, Wichmann, Tuch, Heinrich, & Heyder, 1997). Generally vehicle cabins represent a confined space where passengers are exposed to particulate matter concentrations for variable periods of time. The time spent driving may in some cases significantly contribute to the daily overall body burden, especially with regard to some groups of professional workers such as taxi or bus drivers.

#### 3.4.2. Canteen kitchen

Figure 5 shows very strong fluctuations of the particles' concentration during the measuring period. In the very first part of the concentration profile (from 7:15 a.m. to 8:15 a.m.) the LDSA concentration is around 20 $\mu m^2\ cm^{-3}$, corresponding to a normally polluted indoor environment. A sharp increase was observed with the turning on of the gas stoves (8:15 a.m. to 9:30 a.m.). LDSA concentrations, reaching 1000 $\mu m^2\ cm^{-3}$ and UFP number concentrations of 300.000 $mL^{-1}$, were detected.

A second strong increase in both LDSA concentration and number of ultrafine particles was observed with the turning on of the fryers, at around 10:30 a.m. Here LDSA-concentrations of almost 4000 $\mu m^2\ cm^{-3}$ and UFP number concentrations of 500,000 $mL^{-1}$ were reached. See and Balasubramanian (2006) compared the UFP emission from different gas cooking methods and found that deep-frying generated the largest number of particles and contained the highest proportion of nanoparticles (about 90%). Zhang et al. (Zhang, Gangupomu, Ramirez, & Zhu, 2010) indicated that oil-based cooking (e.g., frying) emitted more UFPs and PM2.5 than water-based cooking (e.g., boiling). Wallace (Wallace, 2006) measured the size

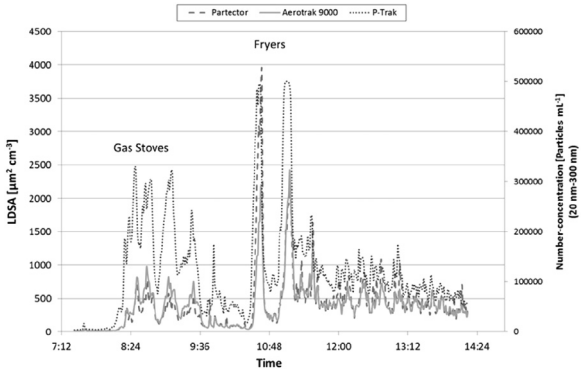


**Fig. 5.** LDSA- and particle number-concentration detected in the canteen's kitchen.

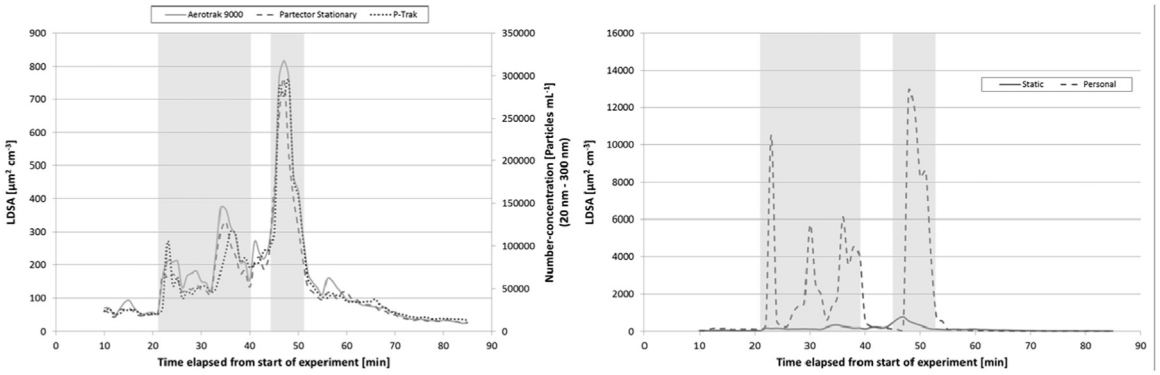


**Fig. 6.** LDSA- and number-concentrations measured while welding. Left: concentrations measured with stationary instruments; right: overlaid stationary and personal LDSA-concentration profiles.

distribution of particles created by frying using cooking oils and found most particles belonging to a size range of 20–40 nm. Average concentrations in the kitchen over the monitored 8-hour period are 400 $\mu m^2\ cm^{-3}$ (LDSA) and 120,000 ultrafine particles $mL^{-1}$. This corresponds to concentrations 20 × (LDSA) and 30 × (UFP particle number) higher compared to typical indoor concentrations of the same metrics. It is noteworthy also that there was a steep increase in temperature during the course of the measuring period starting from 22 °C and ending at 37 °C.

### 3.4.3. *Welding*

Figure 6 shows LDSA-concentrations and number concentration recorded by the stationary instruments located at an approximate distance of 2 m. The areas shaded in grey represent the two welding periods. The background LDSA-concentration is around 80 $\mu m^2\ cm^{-3}$ and therefore around 4 times higher than in typical unpolluted indoor environments. During the two welding episodes LDSA concentrations reached 800 $\mu m^2\ cm^{-3}$ (10 × the background level) while number concentrations reached 300,000 ultrafine particles $mL^{-1}$ (15 × the background level).

Figure 6 (right side) overlays the LDSA-concentrations measured with the stationary Partector and the second Partector, used as a personal sampler analysing air from the breathing zone of the welder. The four concentration peaks can be attributed to when the filler material was closer to the flame with more material evaporating into the air. The air inhaled by the welder reached LDSA-concentrations of approximately 13,000 $\mu m^2\ cm^{-3}$ which, corresponds to 15 × times the concentration measured with the stationary instrument, at the same moment in time. This underlines the importance of conducting personal sampling when assessing exposure instead of relying on stationary measurements which potentially greatly underestimate the concentrations.

It is well known that arc welding generates fumes which are potentially hazardous to health (Albuquerque, Gomes, Pereira, & Miranda, 2015). Welding fumes are metal-containing aerosols consisting of particles formed through complex vaporisation-condensation-oxidation processes during welding (Popović, Prokić-Cvetković, Burzić, Lukić, & Beljić, 2014). Characteristics of the welding fumes depend on a number of welding process parameters such as the type of welding process, the base material composition, the composition of the filler rod, electrical current, arc voltage, the arc length, shielding gas composition/pressure and welding electrode angle (Pires, Quintino, & Miranda, 2007). About 90–95% of the fumes are generated from the filler metal. Since the base metal weld pool is much cooler compared to the electrode tip, its contribution to the overall fume composition is minor (Popović et al., 2014). In the last years, several studies reported on worker exposure to welding fume particles, with particular attention to ultrafine particles. Buonanno et al. (Buonanno,

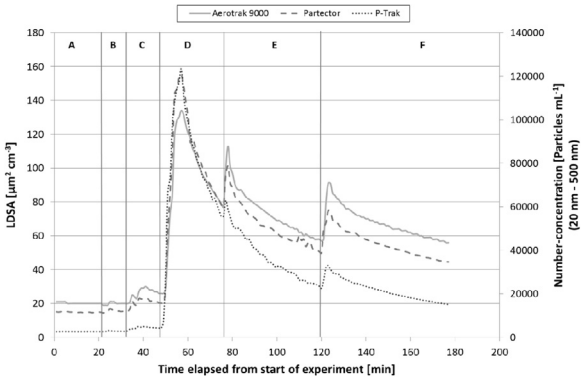


**Fig. 7.** Lung-deposited surface area concentration and number concentration of particles measured in a private house with operational wood-burning stove. A=baseline recording before start of experiment; B=ignition of stove; C=opening of stove due to extinguishing flame; D=boiling of water; E/F=fresh wood billets added to stove.

Morawska, & Stabile, 2011) measured ultrafine particles in the proximity of welding activities in three body shops within automotive plants. They detected LDSA concentrations ranging from 49 to 3200 $\mu m^2\ cm^{-3}$ depending on the site and the welding process (Gas Metal Arc Welding-GMAW in most cases). Number size distribution for GMAW (80% Ar/20% $CO_2$) revealed that the highest amount of particles had an aerodynamic diameter of around 20 nm with a second population of around 150 nm. Guerreiro et al. (2014) characterised particles emitted in the metal active gas welding of carbon steel using mixture of Ar + $CO_2$. He found that the amount of emitted particles (measured by particle number and alveolar deposited surface area) are clearly dependent on the distance to the welding front and also on the main welding parameters, namely the current intensity and heat input in the welding process. With metal active gas (MAG) welding they detected alveolar LDSA concentrations of between 8,325 and 17,574 $\mu m^2\ cm^{-3}$ (AR+10% $CO_2$) and between 22,266 and 42,896 $\mu m^2\ cm^{-3}$ (Ar+18% $CO_2$) and particles with a size of primarily 10–20 nm independently of the gas mixture.

### 3.5. Measurements in non-occupational environments

#### 3.5.1. Private house with wood-burning stove and parallel cooking activities

The aim of this measurement was to assess the impact that operating a wood-burning stove would have on the LDSA concentration in its immediate surroundings. The emission profile depicted in Fig. 7 can be split into 6 sections: section A corresponds to the baseline LDSA- and number-concentration before the stove was lit. At the beginning of section B the stove was lit, pushing some paper under a billet of wood and with the help of a fire-lighter. A barely perceptible increase in the number of particulates in the living room was detected during this operation. A second attempt to light the fire was made since the fire did not flame up properly the first time. To this end the stove door was opened again at the beginning of section C. Smoke released into the living room was detected as can be observed in section C. Since measurements were conducted in a private house, a number of parallel activities were ongoing during the sampling period. At around 50 min after the start of measurements, some water was boiled for cooking with a gas (methane) cooker (section D). This activity led to a sharp increase in the number of detected particles in the living room. The LDSA-concentration increased by approximately 10 times and the number of particles in the size range of between 20 and 500 nm by approximately 50 times.

At the beginning of section E and F fresh billets of wood were added to the wood stove. These events increased the detected LDSA-concentration in the living room by approximately 20–25 $\mu m^2\ cm^{-3}$ and the particles number by approximately 10,000 particles $mL^{-1}$ each.

Results show that each time the wood stove door is opened to add a fresh billet of wood, approximately the equivalent of the baseline LDSA-concentration is released into the investigated environment and added to the baseline concentration. Each time the oven door was opened, the number-concentration of ultrafine particles increased by the equivalent of 3–4 times the baseline concentration.

Although the assessment of emissions from the gas cooker was not the primary objective of this study, it generated much higher amounts, and therefore was a much stronger contributor of ultrafine particles than the wood-burning stove. The LDSA-concentration increased by approximately 7 times and the number concentration by approximately 50 times compared to the baseline measurements. The cooker-fuel (methane) was identified as the predominant source. Water vapour was excluded as the experiment was repeated letting water boil however using an electric stove and, as cross-check, only the gas cooker (the flame without water filled pot) was used. Boiling water contributed only very little ( $< 20\ \mu m^2\ cm^{-3}$ LDSA) to the overall measured concentration whereas the gas stove without the water filled pot immediately increased the LDSA-concentration and number of particles in the living room. Studies conducted in the past (Dennekamp et al., 2001; L'Orange, Volckens, & DeFoort, 2012; Long, Suh, Catalano, & Koutrakis, 2001; Stabile, Fuoco, Marini, & Buonanno, 2015; Wallace, Wang, Howard-Reed, & Persily, 2008; Wallace, Emmerich, & Howard-Reed, 2004) identified cooking as a major source of ultrafine particles indoors. Wallace et al. (2008) studied emission of ultrafine particles from a gas stove flame alone

**Table 2**
Overview table of all measurements conducted.

| Unit | Lung deposited surface area concentration (Aerotrak 9000) [$\mu m^2\ cm^{-3}$] | Lung deposited surface area concentration (Partector) [$\mu m^2\ cm^{-3}$] | Particle number concentration [Part. $mL^{-1}$] | Particles size-distribution | | | | Emission rate [Particles $h^{-1}$] |
|---|---|---|---|---|---|---|---|---|
| | | | | 20–300 nm [%] | 300–400 nm [%] | 400–500 nm [%] | 500–650 nm [%] | |
| Chamber tests | | | | | | | | |
| 3D-Printer | 72[a] | 67[a] | 45,000 | 100 | – | – | – | $6.30 \times 10^{11}$ |
| Incense burning | 872[a] | 633[a] | 142,800 | 99.3 | 0.6 | 0.1 | – | $> 2.10 \times 10^{12}$ |
| Candle burning | 226[a] | 251[a] | 79,390 | 100 | – | – | – | $1.11 \times 10^{12}$ |
| Tobacco cigarette | 1040[a] | 784[a] | 166,283 | 99.0 | 0.8 | 0.2 | – | $> 2.48 \times 10^{12}$ |
| E-cigarette | 11[a] | 8.4[a] | 3822 | 97.8 | 1.0 | 0.6 | 0.4 | $> 5.7 \times 10^{10}$ |
| Occupational environments | | | | | | | | |
| Car journey | N/a | Min: 26.4<br>Max: 277.4<br>Average: 77.2 | N/a | N/a | N/a | N/a | N/a | N/a |
| Canteen kitchen | Min: 17<br>Max: 2427<br>Average: 391 | Min: 15<br>Max: 3927<br>Average: 415 | Min: 3763<br>Max: 500,000<br>Avrg: 123,021 | 99.6 | 0.3 | 0.1 | – | N/a |
| Welding | Min: 22.9<br>Max: 818<br>Average: 160 | Min: 24.7<br>Max: 761<br>Average: 137 | Min: 12,600<br>Max: 294,450<br>Avrg: 55,918 | 100 | – | – | – | N/a |
| Non-occupational environments | | | | | | | | |
| Private house with wood-burning stove and gas cooking | Min: 19<br>Max: 134<br>Average: 61 | Min: 14<br>Max: 151<br>Average: 54 | Min: 2645<br>Max: 123,383<br>Avrg: 29,327 | 99.4 | 0.4 | 0.1 | – | N/a |

[a] Peak concentration.

(no pots or food) and concluded that gas burners emit large numbers of ultrafine particles, smaller than 15 nm in diameter. From their calculated emission rate of $10^{12}$ particles $min^{-1}$ the number of particles in the living room (in our setting) is estimated at approximately $7.4 \times 10^4$ particles $mL^{-1}$. In practice we measured approximately double this concentration. The reason might be attributable to differences in the size of the gas burner and/or the flame temperature. Particulate formation from combustion is linked to processes involving both nucleation and condensation mechanisms (Haynes & Wagner, 1981; Mansurov, 2005). Nucleation begins with the formation of benzene rings through the rearrangement of fragmented chemical chains released during pyrolysis (Fitzpatrick et al., 2008). These rings grow into graphene-like sheets, finally forming stable nuclei. When cooling, the combustion gases then condense onto these nuclei, leading to an increase in their size (L'Orange et al., 2012).

### 3.6. Summary of all measurements

For a better overview, Table 2 summarises all concentrations measured in this study. The table includes LDSA-concentrations measured with both the Aerotrak and the Partector, number concentrations of particles in the size range 20–1000 nm and the size-distribution of the detected particles. For the chamber studies, emission rates are additionally listed.

## 4. Conclusions

The aim of this study was to test a novel handheld instrument under realistic conditions and to collect currently rare LDSA-concentration data in a variety of occupational and non-occupational environments in many of which LDSA-concentrations have never been measured before and which therefore could serve as reference for future studies.

The handheld instrument employed in this study proved to work well both for stationary measurements as well as for personal monitoring and demonstrated to be an alternative to the bulkier bench-instruments. Particles detected in the micro-environments investigated in this study showed to belong predominantly ( $> 99\%$) to a size-range below 300 nm in which diffusion chargers provide a reasonably precise result ( $\pm 30\%$).

Large differences in the particle emissions-rates (in the chamber test) and particle concentrations in the investigated microenvironments were observed. The clearly defined experimental setup in most cases allowed the identification of the particle-source and thus also indirectly the chemical composition. The assessment of toxicity would however require

additional information concerning the characteristics of the measured particulates such as solubility, density and morphology.

## Disclaimers

The content of this work reflects the views of the authors and does not necessarily represent an official position of the European Commission.

## Acknowledgements

The authors thank Ms. Margaret V. Holland for linguistic revision of the manuscript.

## Appendix A. Supplementary material

Supplementary data associated with this article can be found in the online version at http://dx.doi.org/10.1016/j.jaerosci.2016.02.007.

## References

Aitken, R. J., Chaudhry, M. Q., Boxall, A. B., & Hull, M. (2006). Manufacture and use of nanomaterials: current status in the UK and global trends. *Occupational Medicine*, *56*(5), 300–306, http://dx.doi.org/10.1093/occmed/kql051.

Albuquerque, P. C., Gomes, J. F., Pereira, C. A., & Miranda, R. M. (2015). Assessment and control of nanoparticles exposure in welding operations by use of a control banding tool. *Journal of Cleaner Production*, *89*, 296–300, http://dx.doi.org/10.1016/j.jclepro.2014.11.010.

Asbach, C., Fissan, H., Stahlmecke, B., Kuhlbusch, T. A. J., & Pui, D. Y. H. (2009). Conceptual limitations and extensions of lung-deposited nanoparticle surface area monitor (NSAM). *Journal of Nanoparticle Research*, *11*(1), 101–109, http://dx.doi.org/10.1007/s11051-008-9479-8.

ASTM (2011). Standard E741. *Standard test method for determining air change in a single zone by means of a tracer gas dilution*. West Conshohocken, PA: ASTM.

Bau, S., Witschger, O., Gensdarmes, F., & Thomas, D. (2012). Evaluating three direct-reading instruments based on diffusion charging to measure surface area concentrations in polydisperse nanoaerosols in molecular and transition regimes. *Journal of Nanoparticle Research*, *14*(11), 1–17, http://dx.doi.org/10.1007/s11051-012-1217-6.

Behar, R. Z., Hua, M., & Talbot, P. (2015). Puffing topography and nicotine intake of electronic cigarette users. *PLoS One*, *10*(2).

Brook, R. D., Rajagopalan, S., Pope, C. A., Brook, J. R., Bhatnagar, A., Diez-Roux, A., … Metabolism., V. (2010). Particulate matter air pollution and cardiovascular disease: an update to the scientific statement from the american heart association. *Circulation*, *121*(21), 2331–2378, http://dx.doi.org/10.1161/CIR.0b013e3181dbece1.

Brunauer, S., Emmett, P. H., & Teller, E. (1938). Adsorption of gases in multimolecular layers. *Journal of the American Chemical Society*, *60*(2), 309–319, http://dx.doi.org/10.1021/ja01269a023.

Buonanno, G., Marini, S., Morawska, L., & Fuoco, F. C. (2012). Individual dose and exposure of Italian children to ultrafine particles. *Science of the Total Environment*, *438*, 271–277, http://dx.doi.org/10.1016/j.scitotenv.2012.08.074.

Buonanno, G., Morawska, L., & Stabile, L. (2011). Exposure to welding particles in automotive plants. *Journal of Aerosol Science*, *42*(5), 295–304, http://dx.doi.org/10.1016/j.jaerosci.2011.02.003.

Buonanno, G., Morawska, L., Stabile, L., & Viola, A. (2010). Exposure to particle number, surface area and PM concentrations in pizzerias. *Atmospheric Environment*, *44*(32), 3963–3969, http://dx.doi.org/10.1016/j.atmosenv.2010.07.002.

Chang, Y. C., Lee, H. W., & Tseng, H. H. (2007). The formation of incense smoke. *Journal of Aerosol Science*, *38*(1), 39–51, http://dx.doi.org/10.1016/j.jaerosci.2006.09.003.

Chuang, H. C., BéruBé, K., Lung, S. C. C., Bai, K. J., & Jones, T. (2013). Investigation into the oxidative potential generated by the formation of particulate matter from incense combustion. *Journal of Hazardous Materials*, *244–245*, 142–150, http://dx.doi.org/10.1016/j.jhazmat.2012.11.034.

Contos, D. A., Holdren, M. W., Smith, D. L., Brooke, R. C., Rhodes, V. L., & Rainey, M. L. (1995). Sampling and analysis of volatile organic compounds evolved during thermal processing of acrylonitrile butadiene styrene composite resins. *Journal of the Air Waste Management Association*, *45*(9), 686–694, http://dx.doi.org/10.1080/10473289.1995.10467396.

Delfino, R. J., Zeiger, R. S., Seltzer, J. M., & Street, D. H. (1998). Symptoms in pediatric asthmatics and air pollution: differences in effects by symptom severity, anti-inflammatory medication use and particulate averaging time. *Environmental Health Perspectives*, *106*(11), 751–761.

Dennekamp, M., Howarth, S., Dick, C. A., Cherrie, J. W., Donaldson, K., & Seaton, A. (2001). Ultrafine particles and nitrogen oxides generated by gas and electric cooking. *Occupational and Environmental Medicine*, *58*(8), 511–516.

Eeftens, M., Phuleria, H. C., Meier, R., Aguilera, I., Corradi, E., Davey, M., … Tsai, M. Y. (2015). Spatial and temporal variability of ultrafine particles, $NO_2$, $PM_{2.5}$, $PM_{2.5}$ absorbance, $PM_{10}$ and $PM_{coarse}$ in Swiss study areas. *Atmospheric Environment*, *111*, 60–70, http://dx.doi.org/10.1016/j.atmosenv.2015.03.031.

Fierz, M., Meier, D., Steigmeier, P., & Burtscher, H. (2013). Aerosol measurement by induced currents. *Aerosol Science and Technology*, *48*(4), 350–357, http://dx.doi.org/10.1080/02786826.2013.875981.

Fissan, H., Neumann, S., Trampe, A., Pui, D. Y. H., & Shin, W. G. (2007). Rationale and principle of an instrument measuring lung deposited nanoparticle surface area. In A. Maynard, & D. H. Pui (Eds.), *Nanotechnology and occupational health* (pp. 53–59). The Netherlands: Springer.

Fitzpatrick, E., Jones, J., Pourkashanian, M., Ross, A., Williams, A., & Bartle, K. (2008). Mechanistic aspects of soot formation from the combustion of pine wood. *Energy Fuels*, *22*(6), 3771–3778.

Geiss, O., Bianchi, I., Barahona, F., & Barrero-Moreno, J. (2015). Characterisation of mainstream and passive vapours emitted by selected electronic cigarettes. *International Journal of Hygiene and Environmental Health*, *218*(1), 169–180, http://dx.doi.org/10.1016/j.ijheh.2014.10.001.

Gomes, J. F., Bordado, J. C., & Albuquerque, P. C. (2012). On the assessment of exposure to airborne ultrafine particles in urban environments. *Journal of Toxicology Environmental Health A*, *75*(22–23), 1316–1329, http://dx.doi.org/10.1080/15287394.2012.721163.

Guerreiro, C., Gomes, J. F., Carvalho, P., Santos, T. J., Miranda, R. M., & Albuquerque, P. (2014). Characterization of airborne particles generated from metal active gas welding process. *Inhalation Toxicology*, *26*(6), 345–352, http://dx.doi.org/10.3109/08958378.2014.897400.

Haynes, B. S., & Wagner, H. G. (1981). Soot formation. *Progress in Energy and Combustion Science*, *7*(4), 229–273.

Hoek, G., Boogaard, H., Knol, A., De Hartog, J., Slottje, P., Ayres, J. G., … Van Der Sluijs, J. (2010). Concentration response functions for ultrafine particles and all-cause mortality and hospital admissions: results of a European expert panel elicitation. *Environmental Science and Technology*, *44*(1), 476–482, http://dx.doi.org/10.1021/es9021393.

ICRP. (1994). Human respiratory tract model for radiological protection. ICRP publication 66. *Annals of the ICRP*, *24*(1–3).

ISO 12103-1. (1997). *Road vehicles – test dust for filter evaluation – Part 1: Arizona test dust*. Geneva, Switzerland: International Organisation for Standardisation.

ISO 3308. (2012). *Routine analytical cigarette-smoking machine – definitions and standard conditions*. Geneva, Switzerland: International Organisation for Standardisation.

Ji, X., Le Bihan, O., Ramalho, O., Mandin, C., D'Anna, B., Martinon, L., … Pairon, J. C. (2010). Characterization of particles emitted by incense burning in an experimental house. *Indoor Air*, *20*(2), 147–158, http://dx.doi.org/10.1111/j.1600-0668.2009.00634.x.

Kaminski, H., Kuhlbusch, T. A. J., Fissan, H., Ravi, L., Horn, H.-G., Han, H.-S., … Asbach, C. (2012). Mathematical description of experimentally determined charge distributions of a unipolar diffusion charger. *Aerosol Science and Technology*, *46*(6), 708–716, http://dx.doi.org/10.1080/02786826.2012.659360.

Katsouyanni, K., Touloumi, G., Spix, C., Schwartz, J., Balducci, F., Medina, S., … Anderson, H. R. (1997). Short-term effects of ambient sulphur dioxide and particulate matter on mortality in 12 European cities: results from time series data from the APHEA project. Air pollution and health: a European approach. *BMJ*, *314*(7095), 1658–1663.

L'Orange, C., Volckens, J., & DeFoort, M. (2012). Influence of stove type and cooking pot temperature on particulate matter emissions from biomass cook stoves. *Energy for Sustainable Development*, *16*(4), 448–455, http://dx.doi.org/10.1016/j.esd.2012.08.008.

Leavey, A., Fang, J., Sahu, M., & Biswas, P. (2013). Comparison of measured particle lung-deposited surface area concentrations by an Aerotrak 9000 using size distribution measurements for a range of combustion aerosols. *Aerosol Science and Technology*, *47*(9), 966–978, http://dx.doi.org/10.1080/02786826.2013.803018.

Long, C. M., Suh, H. H., Catalano, P. J., & Koutrakis, P. (2001). Using time- and size-resolved particulate data to quantify indoor penetration and deposition behavior. *Environmental Science Technology*, *35*(10), 2089–2099, http://dx.doi.org/10.1021/es001477d.

Mansurov, Z. A. (2005). Soot formation in combustion processes (review). *Combustion, Explosion and Shock Waves*, *41*(6), 727–744, http://dx.doi.org/10.1007/s10573-005-0083-2.

Michaels, R. A., & Kleinman, M. T. (2000). Incidence and apparent health significance of brief airborne particle excursions. *Aerosol Science and Technology*, *32*(2), 93–105, http://dx.doi.org/10.1080/027868200303803.

Mills, N. L., Donaldson, K., Hadoke, P. W., Boon, N. A., MacNee, W., Cassee, F. R., … Newby, D. E. (2009). Adverse cardiovascular effects of air pollution. *Nature Clinical Practice Cardiovascular Medicine*, *6*(1), 36–44, http://dx.doi.org/10.1038/ncpcardio1399.

Morawska, L., He, C., Johnson, G., Jayaratne, R., Salthammer, T., Wang, H., … Wensing, M. (2009). An investigation into the characteristics and formation mechanisms of particles originating from the operation of laser printers. *Environmental Science Technology*, *43*(4), 1015–1022, http://dx.doi.org/10.1021/es802193n.

Moshammer, H., & Neuberger, M. (2003). The active surface of suspended particles as a predictor of lung function and pulmonary symptoms in Austrian school children. *Atmospheric Environment*, *37*(13), 1737–1744, http://dx.doi.org/10.1016/S1352-2310(03)00073-6.

Oberdorster, G., Oberdorster, E., & Oberdorster, J. (2005). Nanotoxicology: an emerging discipline evolving from studies of ultrafine particles. *Environmental Health Perspectives*, *113*(7), 823–839.

Pagels, J., Wierzbicka, A., Nilsson, E., Isaxon, C., Dahl, A., Gudmundsson, A., … Bohgard, M. (2009). Chemical composition and mass emission factors of candle smoke particles. *Journal of Aerosol Science*, *40*(3), 193–208, http://dx.doi.org/10.1016/j.jaerosci.2008.10.005.

Peters, A., Wichmann, H. E., Tuch, T., Heinrich, J., & Heyder, J. (1997). Respiratory effects are associated with the number of ultrafine particles. *American Journal of Respiratory and Critical Care Medicine*, *155*(4), 1376–1383, http://dx.doi.org/10.1164/ajrccm.155.4.9105082.

Pires, I., Quintino, L., & Miranda, R. M. (2007). Analysis of the influence of shielding gas mixtures on the gas metal arc welding metal transfer modes and fume formation rate. *Materials Design*, *28*(5), 1623–1631, http://dx.doi.org/10.1016/j.matdes.2006.02.012.

Popović, O., Prokić-Cvetković, R., Burzić, M., Lukić, U., & Beljić, B. (2014). Fume and gas emission during arc welding: hazards and recommendation. *Renewable and Sustainable Energy Reviews*, *37*, 509–516, http://dx.doi.org/10.1016/j.rser.2014.05.076.

Reche, C., Viana, M., Brines, M., Pérez, N., Beddows, D., Alastuey, A., & Querol, X. (2015). Determinants of aerosol lung-deposited surface area variation in an urban environment. *Science of the Total Environment*, *517*, 38–47, http://dx.doi.org/10.1016/j.scitotenv.2015.02.049.

Rückerl, R., Schneider, A., Breitner, S., Cyrys, J., & Peters, A. (2011). Health effects of particulate air pollution: a review of epidemiological evidence. *Inhalation Toxicology*, *23*(10), 555–592, http://dx.doi.org/10.3109/08958378.2011.593587.

Sager, T. M., & Castranova, V. (2009). Surface area of particle administered versus mass in determining the pulmonary toxicity of ultrafine and fine carbon black: comparison to ultrafine titanium dioxide. *Particle and Fibre Toxicology*, *6* http://dx.doi.org/10.1186/1743-8977-6-15.

SCENIHR (2006). [*Modified opinion (after public consultation) on the appropriateness of existing methodologies to assess the potential risk associated with engineered and adventitious products of nanotechnologies.*].

See, S. W., & Balasubramanian, R. (2006). Physical characteristics of ultrafine particles emitted from different gas cooking methods. *Aerosol and Air Quality Research*, *6*(1), 82–92.

Shin, W. G., Pui, D. Y. H., Fissan, H., Neumann, S., & Trampe, A. (2007). Calibration and numerical simulation of nanoparticle surface area monitor (TSI model 3550 NSAM). *Journal of Nanoparticle Research*, *9*(1), 61–69, http://dx.doi.org/10.1007/s11051-006-9153-y.

Spinazzè, A., Cattaneo, A., Scocca, D. R., Bonzini, M., & Cavallo, D. M. (2015). Multi-metric measurement of personal exposure to ultrafine particles in selected urban microenvironments. *Atmospheric Environment*, *110*, 8–17, http://dx.doi.org/10.1016/j.atmosenv.2015.03.034.

Stabile, L., Fuoco, F. C., & Buonanno, G. (2012). Characteristics of particles and black carbon emitted by combustion of incenses, candles and anti-mosquito products. *Building and Environment*, *56*, 184–191, http://dx.doi.org/10.1016/j.buildenv.2012.03.005.

Stabile, L., Fuoco, F. C., Marini, S., & Buonanno, G. (2015). Effects of the exposure to indoor cooking-generated particles on nitric oxide exhaled by women. *Atmospheric Environment*, *103*, 238–246, http://dx.doi.org/10.1016/j.atmosenv.2014.12.049.

Stephens, B., Azimi, P., El Orch, Z., & Ramos, T. (2013). Ultrafine particle emissions from desktop 3D printers. *Atmospheric Environment*, *79*, 334–339, http://dx.doi.org/10.1016/j.atmosenv.2013.06.050.

Todea, A. M., Beckmann, S., Kaminski, H., & Asbach, C. (2015). Accuracy of electrical aerosol sensors measuring lung deposited surface area concentrations. *Journal of Aerosol Science*, *89*, 96–109, http://dx.doi.org/10.1016/j.jaerosci.2015.07.003.

Unwin, J., Coldwell, M. R., Keen, C., & McAlinden, J. J. (2013). Airborne emissions of carcinogens and respiratory sensitizers during thermal processing of plastics. *Annals of Occupational Hygiene*, *57*(3), 399–406, http://dx.doi.org/10.1093/annhyg/mes078.

Wallace, L. (2006). Indoor sources of ultrafine and accumulation mode particles: size distributions, size-resolved concentrations, and source strengths. *Aerosol Science and Technology*, *40*(5), 348–360, http://dx.doi.org/10.1080/02786820600612250.

Wallace, L., Wang, F., Howard-Reed, C., & Persily, A. (2008). Contribution of gas and electric stoves to residential ultrafine particle concentrations between 2 and 64 nm: size distributions and emission and coagulation remission and coagulation rates. *Environmental Science & Technology*, *42*(23), 8641–8647.

Wallace, L. A., Emmerich, S. J., & Howard-Reed, C. (2004). Source strengths of ultrafine and fine particles due to cooking with a gas stove. *Environmental Science Technology*, *38*(8), 2304–2311.

Waters, K. M., Masiello, L. M., Zangar, R. C., Tarasevich, B. J., Karin, N. J., Quesenberry, R. D., … Thrall, B. D. (2009). Macrophage responses to silica nanoparticles are highly conserved across particle sizes. *Toxicological Sciences*, *107*(2), 553–569, http://dx.doi.org/10.1093/toxsci/kfn250.

Zai, S., Zhen, H., & Jia-song, W. (2006). Studies on the size distribution, number and mass emission factors of candle particles characterized by modes of burning. *Journal of Aerosol Science*, *37*(11), 1484–1496, http://dx.doi.org/10.1016/j.jaerosci.2006.05.001.

Zhang, Q., Gangupomu, R. H., Ramirez, D., & Zhu, Y. (2010). Measurement of ultrafine particles and other air pollutants emitted by cooking activities. *International Journal of Environmental Research and Public Health*, *7*(4), 1744–1759, http://dx.doi.org/10.3390/ijerph7041744.